Research in Astronomy and Astrophysics, 22:045007 (9pp), 2022 April https://doi.org/10.1088/1674-4527/ac51c6

Embedding in Anisotropic Spheres

Alberto K. Mathias[1], Sunil D. Maharaj[2], Jefta M. Sunzu[1], and Jason M. Mkenyeleye[1]
[1] Department of Mathematics and Statistics, The University of Dodoma, P.O. Box 338, Dodoma, Tanzania; jefta@aims.ac.za
[2] Astrophysics Research Centre, School of Mathematics, Statistics and Computer Science, University of KwaZulu-Natal, Durban 4000, South Africa
Received 2021 October 20; revised 2022 January 26; accepted 2022 February 3; published 2022 March 17

Abstract

Exact solutions to the Einstein field equations for class I spacetime symmetry in relativistic stars are generated. The symmetry provides a relation between the gravitational potentials that lead to generalized solutions of the Einstein field equations. We choose one of the gravitational potentials on a physical basis, which allows us to obtain the other gravitational potential via an embedding approach. It is therefore possible to generate a model with astrophysical significance. The model generated satisfies physical properties like stability, causality, regularity, equilibrium and energy conditions.

Key words: gravitation – astroparticle physics – relativistic processes

1. Introduction

Unifying gravitational potentials in astrophysics helps to understand the geometry of spacetime and interior structures of stellar objects. To understand the behavior and physical properties of relativistic objects, the Einstein field equations are essential mathematical tools (Rahaman et al. 2012). Studying the structure and properties of stellar objects is achieved by examining their fluid matter distribution. Schwarzschild (1916) found the first exact solution of the Einstein field equations for astrophysical objects, which opened the way to investigate different models arising from field equations to describe realistic stellar objects. The investigation by Tolman (1939) extended the Schwarzschild model more realistically and connected astrophysical models with data-based facts. The main feature is to consider symmetric properties since this simplifies models to many astrophysical problems. In particular, spacetime symmetry is used to study the nonlinear effects of gravitation and electromagnetic fields. Embedding spacetime into a higher dimensional flat space is a useful approach. Class I spacetime has been used to predict the form of the exact solutions for compact stellar objects (Bhar et al. 2016; Maurya & Govender 2017; Mathias et al. 2021).

Schlaefli introduced the concept of embedding in Euclidean space and indicated that any n-Riemannian manifold V^n could be embedded in an m-dimension pseudo-Euclidean space E^m with $m = \frac{n(n+1)}{2}$ (Singh et al. 2017a). The required extra p dimensions of the pseudo-Euclidean space that embeds V^n in E^m is called the class of the manifold V^n, and must be less than or equal to the number $p = m - n$ or $\frac{n(n-1)}{2}$. For instance, the maximum embedding class p of relativistic spacetime V^4 is 6. Embedding in five-dimensional flat spacetime, class I spacetime, has been successfully used in various extensive studies to model stellar objects. The embedding approach gives additional differential equations named the Karmarkar condition (Maurya & Maharaj 2018). Therefore, the Karmakar condition helps to solve the Einstein field equations.

Research in relativistic astrophysics includes pressure anisotropy as an important ingredient in modeling systems of compact stellar objects. This is important in finding physical solutions of the Einstein field equations that describe realistic stars (Stephani et al. 2003). Bowers & Liang (1974) discussed the importance of local anisotropy in relativistic fluid models. Furthermore, Herrera & Santos (1997) addressed the impact of local anisotropy in the matter distribution and suggested its inclusion for several physical processes in compact astrophysical objects with large density of about $10^{15}\,\mathrm{g\,cm^{-3}}$. Dev & Gleiser (2002) demonstrated that pressure anisotropy in stellar objects is associated with mass, structure and redshift which can all change for different values of the magnitude of anisotropy. Other research describing the physical effect of anisotropy and verifying the significance of non-zero anisotropy in modeling stellar objects has been conducted by Lighuda et al. (2021), Maurya & Maharaj (2017), Murad (2016), Murad & Fatema (2015), Ngubelanga et al. (2015), Sharma & Ratanpal (2013), Sunzu et al. (2014a, 2014b), and Sunzu et al. (2019).

In general relativity, more researchers on symmetry of class I spacetimes have considered the additional restrictions on gravitational potentials (Gedela et al. 2018; Pandya & Thomas 2019). Models that incorporate embedding show that the Karmarkar condition allows one to choose forms of gravitational potentials to develop new stellar models as described by Maurya & Govender (2017), Murad (2018) and Maurya & Maharaj (2017). In seeking a generalized solution to the Einstein field equations with spherical symmetry when implementing the Karmarkar condition, we impose restrictions on the metric functions. We specify the gravitational potential $z(x)$ on a physical basis. Then, through the Karmarkar condition we obtain the other gravitational potential

$y(x)$ by applying the integrability condition. This enables us to solve the Einstein field equations by generating a model that fully describes the behavior of relativistic stars. The solutions obtained are used to examine the applicability of the physical boundary conditions of compact stars.

2. Einstein Field Equations

The Einstein field equations describe the gravitational behavior of astrophysical objects. This is done by considering the spacetime local coordinates $(x^i) = (t, r, \theta, \phi)$ whose interior line element takes the Schwarzschild form

$$ds^2 = -e^{\nu(r)}dt^2 + e^{\lambda(r)}dr^2 + r^2(d\theta^2 + \sin^2\theta d\phi^2), \quad (1)$$

where $\nu(r)$ and $\lambda(r)$ are functions for the gravitational potentials. The exterior Schwarzschild spacetime for a relativistic fluid sphere takes the form

$$ds^2 = -\left(1 - \frac{2M}{r}\right)dt^2 + \left(1 - \frac{2M}{r}\right)^{-1}dr^2 + r^2(d\theta^2 + \sin^2\theta d\phi^2), \quad (2)$$

where M stands for the total mass of the stellar object. The Einstein field equations for the distribution of anisotropic fluids are given by

$$8\pi\tau^i_j = R^i_j - \frac{1}{2}Rg^i_j, \quad (3)$$

where τ^i_j and R^i_j are respectively the energy momentum tensor and the Ricci tensor, and R represents the scalar curvature. The energy momentum tensor for the distribution of anisotropic matter is evident in models of Maurya & Maharaj (2017) and Bhar et al. (2017b) given by

$$\tau^i_j = \rho\upsilon^i\upsilon_j + p_r\chi_j\chi^i + p_t(\upsilon^i\upsilon_j - \chi_j\chi^i - g^i_j), \quad (4)$$

where the contravariant quantity υ^i is the four-velocity vector and χ^i is the unit spacelike vector in the radial direction. The quantities ρ, p_r and p_t stand for matter density, radial pressure and tangential pressure respectively.

In view of the line element (1) together with (3) and (4), the anisotropic field equations become

$$8\pi\rho(r) = \frac{1 - e^{-\lambda}}{r^2} + \frac{e^{-\lambda}\lambda'}{r}, \quad (5a)$$

$$8\pi p_r(r) = \frac{\nu' e^{-\lambda}}{r} - \frac{1 - e^{-\lambda}}{r^2}, \quad (5b)$$

$$8\pi p_t(r) = \frac{e^{-\lambda}}{4}\left(2\nu'' + \nu'^2 - \nu'\lambda' + \frac{2\nu'}{r} - \frac{2\lambda'}{r}\right), \quad (5c)$$

$$\Delta = 8\pi(p_t - p_r) = e^{-\lambda}\left(\frac{\nu''}{2} + -\frac{\nu'\lambda'}{4} + \frac{\nu'^2}{4} - \frac{\nu' + \lambda'}{2r} + \frac{e^{\lambda} - 1}{r^2}\right). \quad (5d)$$

The primes indicate differentiation with respect to the radial distance r and Δ stands for the pressure anisotropy. For isotropic pressure $\Delta = 0$, $p_t = p_r$. Geometrized units are employed in which the coupling constant and the velocity of light are regarded as unity ($G = c = 1$).

3. Class I Condition

Embedding of spacetimes can be used to generate models for compact stellar objects. The fundamental symmetric tensor $b_{\mu\beta}$ satisfying the necessary and sufficient Gauss–Codazzi conditions for embedding four-dimensional spacetime into higher dimensional Euclidean space is described by Eisenhart (1966). They are given by the equations

$$R_{\mu\nu\alpha\beta} = \epsilon(b_{\mu\alpha}b_{\nu\beta} - b_{\mu\beta}b_{\nu\alpha}), \quad (6a)$$

$$0 = b_{\mu\nu;\alpha} - b_{\mu\alpha;\nu}, \quad (6b)$$

where $\epsilon = \pm 1$ and semicolons stand for covariant differentiation. Riemann curvature tensor components with non-zero values are obtained from the line element (1). This helps to generate the non-zero values of the fundamental form $b_{\mu\alpha}$ corresponding to Equation (1). The non-zero components of the Riemann curvature tensor include

$$R_{1414} = -e^{\nu}\left(\frac{\nu''}{2} + \frac{\nu'^2}{4} - \frac{\lambda'\nu'}{4}\right), \quad (7a)$$

$$R_{2323} = -e^{\lambda}r^2\sin^2\theta\,(e^{\lambda} - 1), \quad (7b)$$

$$R_{1212} = \frac{1}{2}r\,\lambda', \quad (7c)$$

$$R_{3434} = -\frac{1}{2}\sin^2\theta\,\nu' e^{\nu - \lambda}. \quad (7d)$$

The non-zero components of the symmetric tensor $b_{\mu\beta}$ corresponding to Equation (1) include b_{11}, b_{22}, b_{33} and b_{14} with $b_{33} = b_{22}\sin^2\theta$. Then, incorporating all the non-zero components, Equation 6(a) gives the relation

$$R_{1414} = \frac{R_{1212}R_{3434} + R_{1224}R_{1334}}{R_{2323}}, \quad (8)$$

which is known as the Karmarkar condition (Karmarkar 1948). For class I spacetimes, Equation 6(a) must satisfy $R_{2323} \neq 0$ (Pandey & Sharma 1982; Singh et al. 2017b). The embedding process essentially maps the four-dimensional spacetime into a higher dimensional Minkowski space. Consequently the light cone structure of the manifold is mapped into flat spacetime and may be interpreted in these terms.

Substituting (7) into (8) leads to the nonlinear differential equation

$$\frac{\lambda' e^{\lambda}}{e^{\lambda} - 1} = \frac{2\nu''}{\nu'} + \nu', \quad (9)$$

which can be solved to provide an equation relating the gravitational potentials $\nu(r)$ and $\lambda(r)$. This is given by

$$e^{\frac{\nu}{2}} = C + H\int \sqrt{(e^{\lambda(r)} - 1)}\,dr, \tag{10}$$

where C and H are constants of integration.

4. A Transformation

To obtain solutions for the Einstein field equations via the embedding approach, we first transform the system (5). The transformation of the system (5) is equivalent to that of Durgapal & Bannerji (1983). This is done by introducing the independent variable x and new metric functions y and z defined as

$$x = C_1 r^2, \quad z(x) = e^{-\lambda(r)}, \quad y(x) = e^{\nu(r)}. \tag{11}$$

With Equation (11), the system expressed in Equation (5) becomes

$$8\pi\rho(x) = C_1\left(\frac{1-z}{x} - 2\,\dot{z}\right), \tag{12a}$$

$$8\pi p_r(x) = C_1\left(2\,z\,\frac{\dot{y}}{y} - \frac{1-z}{x}\right), \tag{12b}$$

$$8\pi p_t(x) = C_1\left(2x\,z\,\frac{\ddot{y}}{y} + (2\,z + x\,\dot{z})\,\frac{\dot{y}}{y} - x\,z\,\frac{\dot{y}^2}{y^2} + \dot{z}\right), \tag{12c}$$

$$8\pi\Delta = C_1\left(z\left(2x\,\frac{\ddot{y}}{y} - x\frac{\dot{y}^2}{y^2}\right) + \dot{z}\left(1 + x\frac{\dot{y}}{y}\right) - \frac{1-z}{x}\right), \tag{12d}$$

where dots denote differentiation with respect to x. When $\Delta = 0$, the pressure becomes isotropic.

5. Generating a New Model

In generating a new model, we apply the solution of the nonlinear differential equation obtained from embedding spacetime into flat space as shown in (10). Expressing the solution (10) in terms of the transformed variables x, y and z, we obtain an equivalent equation given as

$$y(x) = \left(C + \frac{1}{2}H\int \sqrt{\frac{1-z}{xz}}\,dx\right)^2. \tag{13}$$

Studies in general relativity use different techniques when describing the properties and structure of stellar bodies. The approach of transforming the field Equations (5) has been done by several researchers applying different techniques. Manjonjo et al. (2018, 2019) imposed conformal symmetry on the spacetime manifold. The conformal Killing vector was used with the Einstein field equation to provide a relationship between gravitational potentials. Also, Matondo et al. (2018) generated realistic stellar models by incorporating the conformal Killing vector into the Einstein field equations. Another technique is to use equations of state relating the energy density and the pressure of the stellar object. Maharaj et al. (2014) and Sunzu et al. (2014a, 2019) utilized the linear equation of state. Sunzu & Mashiku (2018) adopted the quadratic equation of state to generate exact solutions. The Van der Waals equation of state was applied by Thirukkanesh & Ragel (2012) where the metric function z is specified.

In generating stellar models, previous research on class I spacetime limited only the forms of gravitational potentials e^{λ} and e^{ν}. This is shown in models by Arkani-Hamed et al. (1998), Baskey et al. (2021), Bhar (2015), Bhar et al. (2015, 2017a), Errehymy et al. (2021) and Maharaj & Govender (2005). This approach is useful in solving the Einstein field equations. In this work, the field equations are transformed, and the Karmarkar condition is applied to provide an equation relating the gravitational potentials. For class I spacetimes, the approach of transforming the field equations and Karmarkar condition has not been employed before.

All physical quantities in the system (12) are defined in terms of three partial differential equations with five unknown variables $\lambda(x)$, $\nu(x)$, $\rho(x)$, $p_r(x)$ and $p_t(x)$. Conditions with physical significance on the distribution of matter in the system (12) such as regularity and stability will limit choices made for the gravitational potential $\lambda(x)$. To solve system (12), we first need to integrate Equation (13) by specifying the gravitational potential $z(x)$. We choose the gravitational potential $z(x)$ to be

$$z(x) = \frac{1}{1+x}. \tag{14}$$

The motivation behind choosing this form of gravitational potential is to generalize the particular solutions obtained from previous works. The choice is regular and continuous throughout the interior of the stellar object. Particular solutions with similar choices of gravitational potential have been generated using equations of state. These are found in the Finch & Skea (1989) model for a linear equation of state. In our work, we utilize the Karmarkar condition with the choice of metric functions (14) to generate general exact solutions to the Einstein field equations with embedding into Euclidean space. Using Equations (13) and (14), we have

$$y(x) = \frac{(2C + H(A_1 + x))^2}{4}, \tag{15}$$

where A_1 is a constant of integration.

Using Equations (14) and (15), the matter variables and the gravitational potentials in Equation (12) become

$$e^{\nu}(x) = \frac{(2C + H(A_1 + x))^2}{4}, \tag{16a}$$

$$e^{\lambda}(x) = 1 + x, \tag{16b}$$

$$\rho(x) = \frac{C_1(3+x)}{8\pi(1+x)^2}, \tag{16c}$$

$$p_r(x) = -\frac{C_1(2C + H(-4+A_1+x))}{8\pi(1+x)(2C+H(A_1+x))}, \tag{16d}$$

$$p_t(x) = \frac{C_1(-2C + H(4-A_1+x))}{8\pi(1+x)^2(2C+H(A_1+x))}, \tag{16e}$$

$$p_t(x) - p_r(x) = \Delta = \frac{C_1 x(2C + H(-2+A_1+x))}{8\pi(1+x)^2(2C+H(A_1+x))}, \tag{16f}$$

where C, H and A_1 are real constants and should be chosen such that $\rho(x) \geqslant 0$, $p_t(x) \geqslant 0$, $p_r(x) \geqslant 0$ and $e^{\nu} > 0$. In this case some constants may take negative values (A_1, C, $H < 0$). This is also discussed in Section 6. However, in our case the anisotropy is nonzero which allows for a wider range of behavior as shown in Thirukkanesh & Maharaj (2008). The solution in (16) describes the feature of anisotropic stellar objects in the absence of an electric field. The solution in (16) is for the system of field equations in (12) which were formulated by transforming the field equations in (5). These equations were also used by Schwarzchild to generate the first particular solution describing compact astrophysical objects. The system (16) describes a solution to the Einstein field equations which utilizes the embedding approach of class I spacetime. These complement earlier treatments (Maurya & Govender 2017; Murad 2018; Bhar 2019).

6. Analysis of the Physical Properties

The system (16) satisfies several physical conditions that are appropriate for the behavior of an astrophysical object. These conditions include regularity, stability, causality, energy conditions, equilibrium, mass–radius relation and matching conditions.

6.1. Regularity Condition

The regularity of the fluid anisotropic model is assessed by observing if the model is free from physical and geometric singularities. It is observed in Figures 1 and 2 that at the center ($r = 0$), the metric potentials have the values $e^{\nu} > 0$ and $e^{-\lambda} = 1$ respectively. This demonstrates that the metric potentials in the star's interior are regular, non-negative and finite. In addition, the metric potential $e^{-\lambda}$ is monotonically decreasing toward the surface. Similar profiles to this form of the gravitational potential were obtained by Bhar et al. (2017b, 2017c) and Singh et al. (2017a).

The essential aspects also shown in the new model are the profiles of the matter variables ρ, p_r and p_t being non-negative and monotonically decreasing as they approach the surface of the star. The sketches of these matter variables from Figures 3–5 affirm that the values at the center are at the highest points.

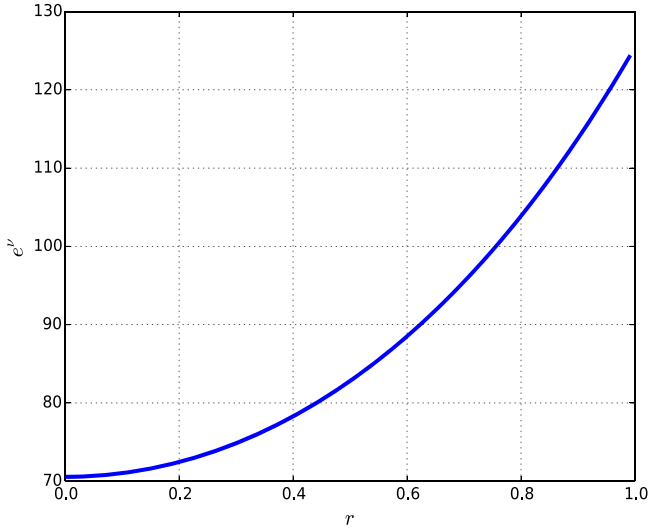

Figure 1. Potential e^{ν} vs. radial interval.

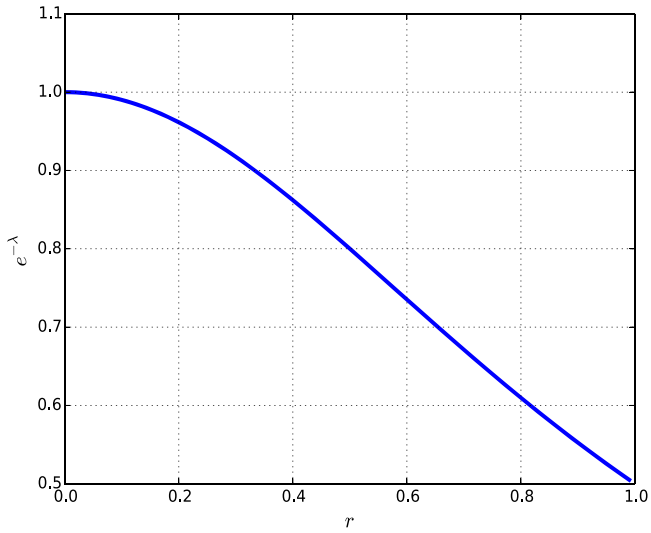

Figure 2. Potential $e^{-\lambda}$ vs. radial interval.

6.2. Stability Through Adiabatic Condition

The stability of the model is described by considering the adiabatic index Γ. For an isotropic model, Γ should satisfy the condition

$$\Gamma = \left(\frac{\rho + p_r}{p_r}\frac{dp_r}{d\rho}\right) > \frac{4}{3}. \tag{17}$$

Effective models in general relativity, with anisotropic pressures, play a critical role in analyzing the stability of the model. Stability of the anisotropic model is tested as indicated

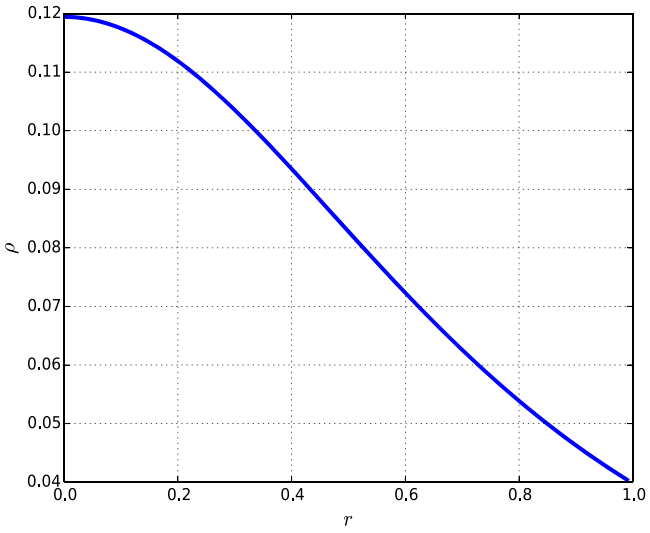

Figure 3. Energy density vs. radial interval.

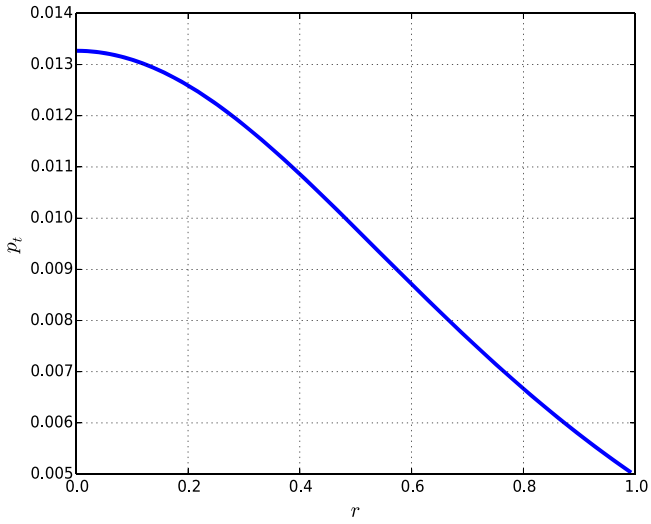

Figure 5. Tangential pressure against radial distance.

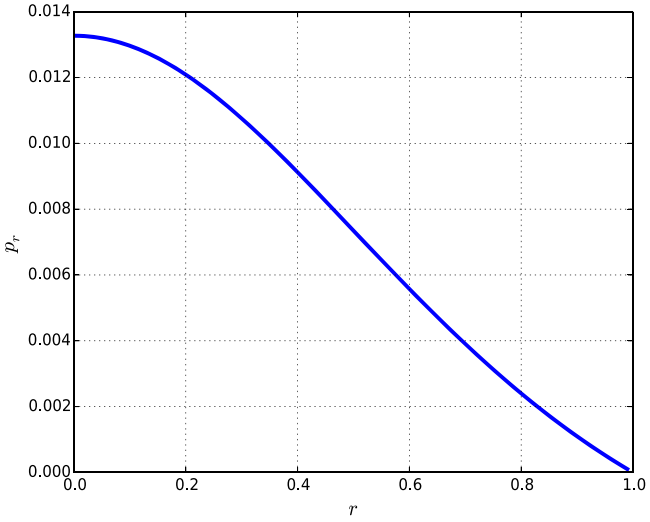

Figure 4. Radial pressure vs. radial interval.

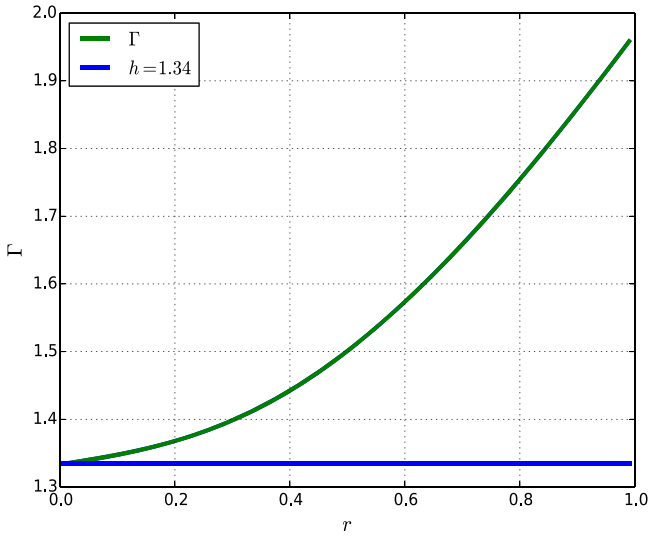

Figure 6. Stability vs. radial interval.

in the paper by Maurya & Maharaj (2017) given by

$$\Gamma > \frac{4}{3}\left[1 + 3\pi\frac{\rho_0\, p_{r0}\, r}{|p'_{r0}|} + \frac{p_{r0} - p_{t0}}{r\,|p'_{r0}|}\right], \tag{18}$$

where the subscript 0 represents central values. From Figure 6 we observe that the adiabatic index satisfies the condition $\Gamma > \frac{4}{3}$ everywhere inside the compact star.

6.3. Causality Condition

Causality requires the speed of sound inside the stellar interior to be less than the speed of light. The tangential and radial speeds of the model in (16) are given by the formula

$$v_r^2 = \frac{dp_r}{d\rho}, \quad v_t^2 = \frac{dp_t}{d\rho}.$$

It is observed from Figure 7 that the speed of sound increases monotonically away from the center with $v_t^2 < 1$ and $v_r^2 < 1$. This behavior obeys the structure of realistic stellar models. Similar structure is also observed in the work of Maharaj & Mafa Takisa (2012), Maurya & Govender (2017) and Maurya & Maharaj (2018).

We have also used the concept of cracking to examine the stability of our anisotropic model as introduced by Herrera

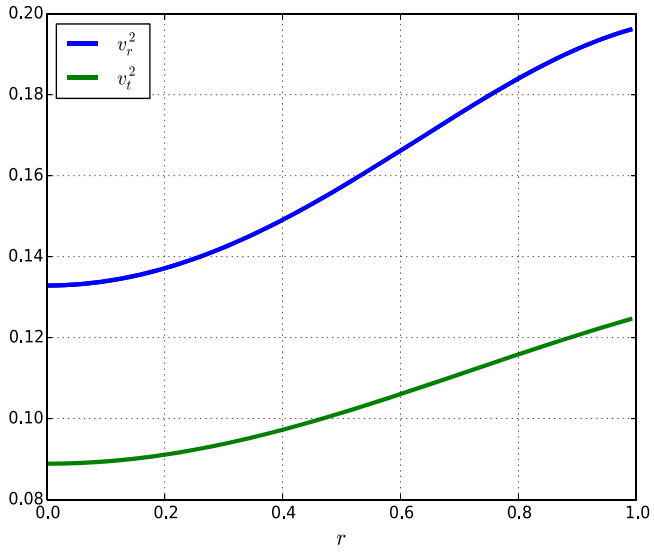

Figure 7. Sound of speed vs. radial interval.

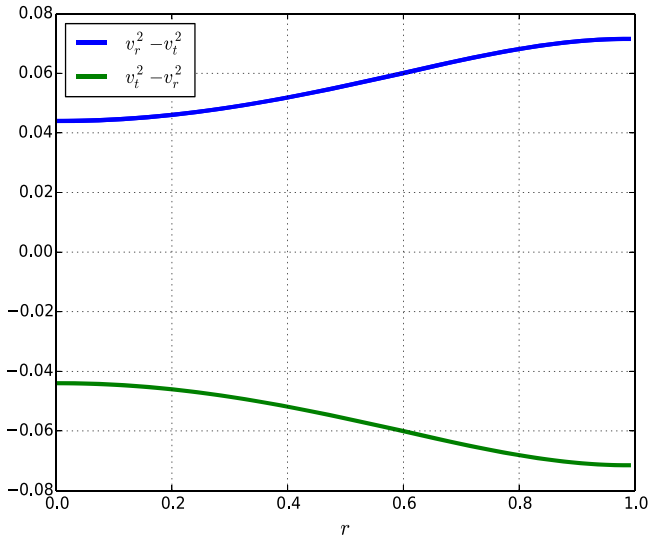

Figure 8. Criterion of cracking vs. radial interval.

(1992). Abreu et al. (2007) showed that the anisotropic fluid distribution of matter is potentially stable if the radial pressure is larger compared to tangential pressure with $0 < v_r^2 - v_t^2 < 1$ and $-1 < v_t^2 - v_r^2 < 0$. With the help of graphical representation in Figure 8, our anisotropic model is stable. This is in agreement with the model generated by Maurya & Maharaj (2018).

6.4. Energy Conditions

A realistic stellar model should satisfy the energy conditions that include null energy condition (NEC), weak energy condition (WEC), strong energy condition (SEC) and dominant energy condition (DEC). Any realistic physical model must satisfy the following energy conditions

$$\begin{aligned} \text{NEC:}\ & \rho > 0, \\ \text{WEC:}\ & \rho - p_t \geqslant 0,\ \rho - p_r \geqslant 0, \\ \text{SEC:}\ & \rho - 2p_t - p_r \geqslant 0, \\ & \rho - 3p_r \geqslant 0,\ \rho - 3p_t \geqslant 0, \\ \text{DEC:}\ & \rho - |p_t| \geqslant 0,\ \rho - |p_r| \geqslant 0 \end{aligned}$$

(Jape et al. 2021). From Figures 9 and 10 it is clear that our model satisfies all conditions for energy within the stellar interior.

6.5. Equilibrium Conditions

The equilibrium condition of the model is examined by considering different forces. The generalized Tolman–Oppenheimer–Volkoff (TOV) equation describes the equilibrium condition for anisotropic fluid distributions (Tolman 1939)

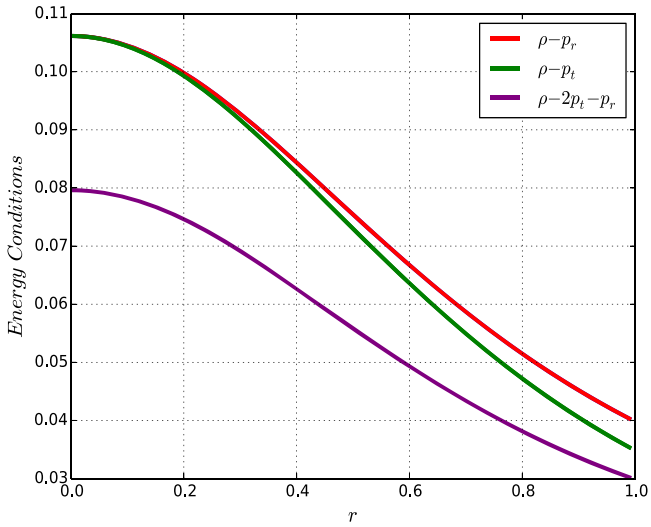

Figure 9. Energy condition vs. radial interval.

given by

$$\frac{2\Delta}{r} = \frac{dp_r}{dr} + \frac{m_g(\rho + p_r)}{r^2} e^{\frac{\lambda-\nu}{2}}, \tag{19}$$

where $m_g(r)$ is the effective gravitational mass. The equilibrium condition is determined by the equation

$$F_a + F_g + F_h = 0, \tag{20}$$

where F_a is anisotropic force, F_g is gravitational force and F_h is hydrostatic force. We obtain different but equivalent forms for

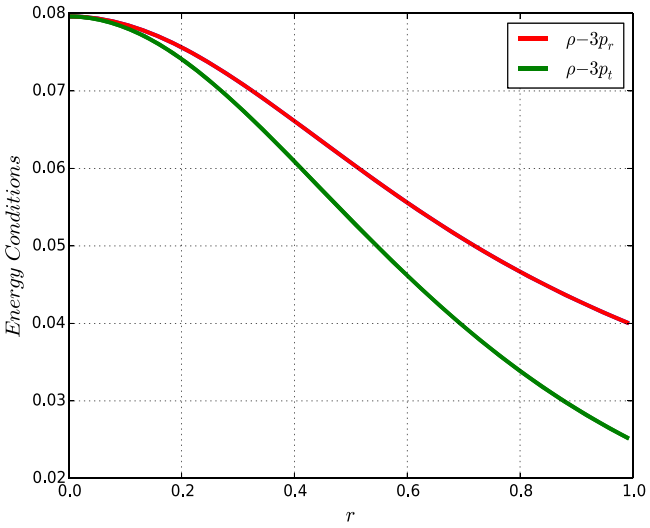

Figure 10. Energy condition vs. radial distance.

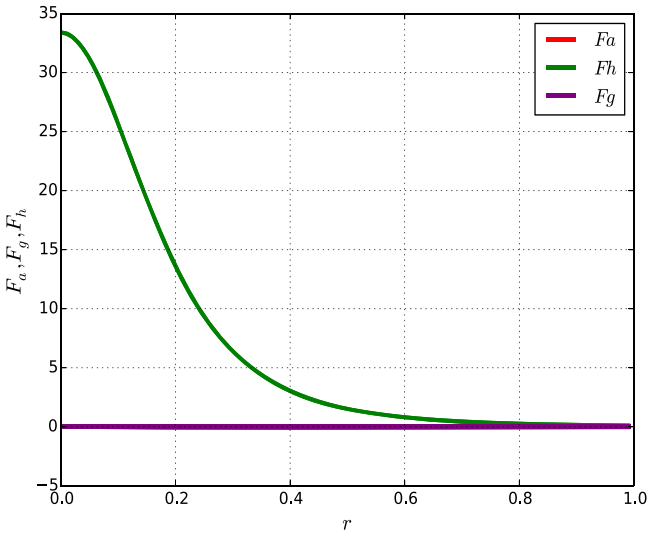

Figure 11. Forces vs. radial interval.

$m_g(r)$, F_a, F_g and F_h in terms of variables in Equation (11) as

$$m_g(x) = x^{\frac{3}{2}} y^{\frac{1}{2}} z^{\frac{1}{2}} \frac{\dot{y}}{y},$$
$$F_g = m_g(x) \frac{(\rho + p_r(x))}{x} y^{\frac{1}{2}} z^{\frac{1}{2}},$$
$$F_h = -\frac{dp_r(x)}{dx},$$
$$F_a = \frac{2\Delta}{x^{\frac{1}{2}}}.$$

The sum of these three forces satisfies Equation (20) as indicated in Figure 11.

6.6. Mass–Radius Relation

For any physically valid star model, according to Buchdahl (1959), the ratio of mass to radius must satisfy the condition $\frac{2M}{r} < \frac{8}{9}$. Mak & Harko (2003) defined a generalized relationship to find the ratio of mass to radius given by

$$M(x) = \frac{k}{2} \int_0^x \rho(y) y^{\frac{1}{2}} dy,$$
$$= \frac{C_1 x^{\frac{3}{2}}}{(1+x)}. \quad (21)$$

The above mass function satisfies the properties of the physical star model for a compact astrophysical object, and this is verified in Figure 12.

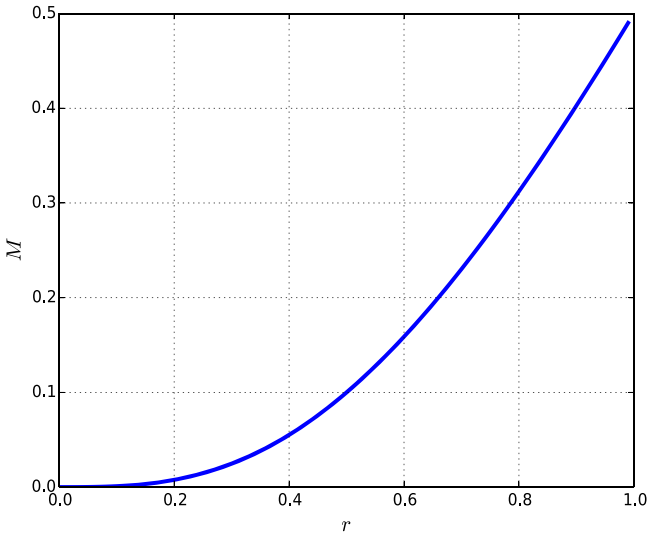

Figure 12. Mass vs. radial interval.

6.7. Matching Condition

We consider the exact solutions from the new model by matching the solution of interior line element (1) and exterior line element (2) at the surface of the star. The matching condition is determined as indicated in Thirukkanesh & Ragel (2012). This is done by taking $r = R$ at the boundary. Then Equations (1) and (2) give

$$e^{\lambda} = \left(1 - \frac{2M}{R}\right)^{-1}, \quad (22a)$$

$$e^{\nu} = 1 - \frac{2M}{R}. \tag{22b}$$

In g_{00}, substituting Equation (14) into Equation 22(a), we obtain the constant C_1 in terms of M and R,

$$C_1 = \frac{2M}{R^2(R-2M)}. \tag{23}$$

In g_{11}, substituting Equation (15) into Equation 22(b), we obtain the constant of integration C in terms of C_1, M and R

$$C = \left(1 - \frac{C_1 R^2}{4}\right)\left(\sqrt{1 - \frac{2M}{R}}\right). \tag{24}$$

With Equations (23) and (24), we can obtain C in terms of M and R as

$$C = \left(1 - \frac{M}{2(R-2M)}\right)\left(\sqrt{1 - \frac{2M}{R}}\right). \tag{25}$$

Vanishing of the radial pressure at the boundary $p_{(r=R)} = 0$ gives the constant of integration H in terms of M and R

$$H = \frac{1}{2}\left(\sqrt{1 - \frac{2M}{R}}\right). \tag{26}$$

Matching of the exact solutions is represented by Equations (23), (25) and (26). The constants C and H are expressed in terms of M and R.

7. Discussion

In this paper, our objective was to extend the characteristics of the embedding approach to the solution of stellar bodies. This is done by the transformation of matter variables in the system (12) so as to form a new exact solution to the Einstein field equations. The Karmarkar condition provides a relation between the metric potentials $y(x)$ and $z(x)$. This generates a new exact solution by choosing the gravitational potential $z(x)$ on a physical basis. By doing this, a model with acceptable behavior is developed as indicated in the system (16). The analysis of the generated model is established through graphical representation using the Python programming language for the following constants: $H = 5.6$, $C = -14$ and $A_1 = 8$.

The representation in the graphs for the metric functions $(e^{-\lambda}, e^{\nu})$ and the matter variables shows that ρ, p_r and p_t are well behaved inside the stellar object as given in Figures 1–5. In this model, we have demonstrated that the stability condition through adiabatic index is satisfied as $\Gamma > \frac{4}{3}$ (Maurya & Maharaj 2018). This is clearly seen in Figure 6. Stability of the model can also be examined by using the speed of sound and speed of light; this feature is known as the causality condition. The tangential and radial speed of sound must either be monotonically decreasing or increasing and does not exceed the speed of light, that is v_r^2, $v_t^2 < 1$ (Abreu et al. 2007). Moreover,

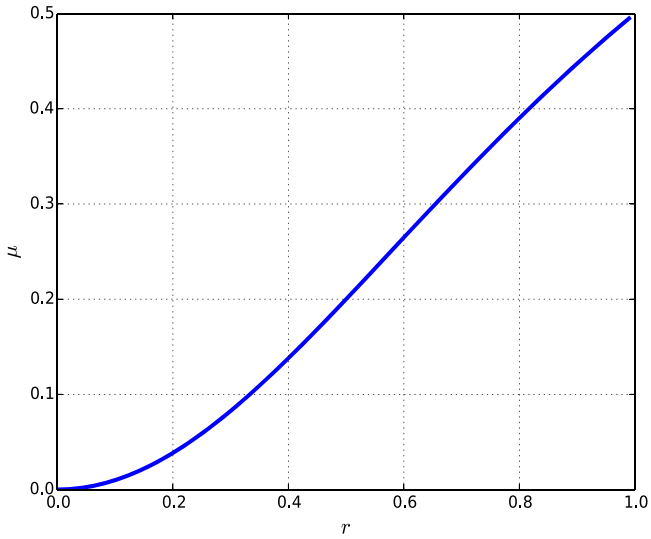

Figure 13. Compactness vs. radial interval.

if the tangential speed of sound is greater than the radial speed of sound, then the model is potentially stable, that is $v_t^2 - v_r^2 < 1$; this method is known as the "cracking method." Figures 7 and 8 indicate that all the necessary causality properties for an astrophysical object are satisfied.

Our generated model satisfies the energy conditions, which are strong, weak, dominant and null, as displayed in Figures 9 and 10. Furthermore the equilibrium condition by TOV is verified by the addition of the anisotropic force, hydrostatic force and gravitational force, and its sketch is depicted in Figure 11. The exact solutions developed in system (16) are well behaved since the properties and structure of the relativistic star model like mass and compactness increase monotonically, similar to the works by Hansraj (2017), Moopanar & Maharaj (2013) and Singh et al. (2017b). The plots for mass and compactness of the model are shown in Figures 12 and 13, respectively. The anisotropy is monotonically increasing and consistent with the physical requirement of relativistic stars. This can be clearly seen in Figure 14. We obtain an exact solution which is free from physical singularities as $e^{\nu(x)} > 0$, $e^{-\lambda(x)} > 0$, $0 \leqslant p_r(x) < \infty$, $0 \leqslant p_t(x) < \infty$, $0 \leqslant \rho(x) < \infty$ in the range of radius $0 \leqslant x < 1$.

To this end, in our embedding study, we have observed that the use of class I spacetime or the Karmarkar condition into Euclidean flat space leads to a new exact solution. This was achieved by making a simple choice for a variable $z(x)$ in (13). Other potential $z(x)$ choices could also lead to physically interesting models.

The exact solution (16) is given in terms of elementary functions. It is therefore possible to find the physical quantities of observational interest such as stellar masses, stellar radii,

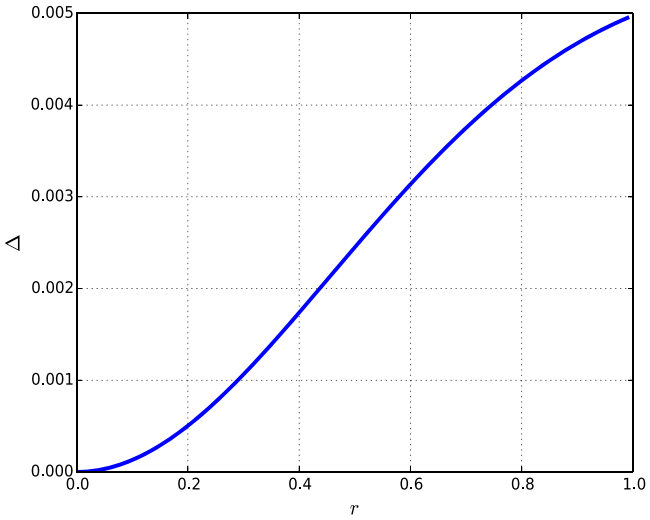

Figure 14. Measure of anisotropy vs. radial interval.

luminosities and surface redshifts. The values obtained can be compared with known astronomical objects as prepared by Gedela et al. (2019) and Bisht et al. (2021).

Acknowledgments

We are thankful to the University of Dodoma in Tanzania for the continuous support and encouragement to complete this research work. A.K.M. is grateful to the Ministry of Education, Science and Technology of Tanzania for sponsorship. S.D.M. acknowledges gratitude to the South African Research Chair Initiative of the Department of Science and Technology and the National Research Foundation that facilitate the research funding.

ORCID iDs

Sunil D. Maharaj https://orcid.org/0000-0002-1967-2849
Jefta M. Sunzu https://orcid.org/0000-0002-8780-3927

References

Abreu, H., Hernandez, H., & Nunez, L. A. 2007, CQGra, 24, 4631
Arkani-Hamed, N., Dimopoulos, S., & Dvali, G. 1998, PhLB, 429, 263
Baskey, L., Das, S., & Rahaman, F. 2021, MPLA, 36, 2150028
Bhar, P. 2015, Ap&SS, 359, 41
Bhar, P. 2019, EPJC, 79, 138
Bhar, P., Govender, M., & Sharma, R. 2017a, EPJC, 77, 109
Bhar, P., Maurya, S. K., Gupta, Y. K., & Manna, T. 2016, EPJA, 52, 312
Bhar, P., Rahaman, F., Ray, S., & Chatterjee, V. 2015, EPJC, 75, 190
Bhar, P., Singh, K. N., & Manna, T. 2017b, IJMPD, 26, 1750090
Bhar, P., Singh, K. N., & Pant, N. 2017c, InJPh, 91, 701
Bisht, R. K., Gedela, S., Pant, N., & Tewari, N. 2021, RAA, 21, 162
Bowers, R. L., & Liang, E. P. T. 1974, ApJ, 188, 657
Buchdahl, H. A. 1959, PhRv, 116, 1027
Dev, K., & Gleiser, M. 2002, GReGr, 34, 1793
Durgapal, M. C., & Bannerji, R. 1983, PhRvD, 27, 328
Eisenhart, L. P. 1966, Riemannian Geometry (6th edn; Princeton, NJ: Princeton Univ. Press)
Errehymy, A., Khedif, Y., & Daoud, M. 2021, EPJC, 81, 266
Finch & Skea 1989, CQGra, 6, 467
Gedela, S., Bisht, R. K., & Pant, N. 2018, EPJA, 54, 207
Gedela, S., Pant, N., Upreti, J., & Pant, R. P. 2019, EPJC, 79, 566
Hansraj, S. 2017, EPJC, 77, 557
Herrera, L. 1992, PhLA, 165, 206
Herrera, L., & Santos, N. O. 1997, PhR, 286, 53
Jape, J. W., Maharaj, S. D., Sunzu, J. M., & Mkenyeleye, J. M. 2021, EPJC, 81, 1057
Karmarkar, K. R. 1948, Proc. Indian Acad. Sci. A, 27, 56
Lighuda, A. S., Sunzu, J. M., Maharaj, S. D., & Mureithi, E. W. 2021, RAA, 21, 310
Maharaj, S. D., & Govender, M. 2005, IJMPD, 14, 667
Maharaj, S. D., & Mafa Takisa, P. 2012, GReGr, 44, 1419
Maharaj, S. D., Sunzu, J. M., & Ray, S. 2014, EPJP, 129, 3
Mak, M. K., & Harko, T. 2003, RSPSA, 459, 393
Manjonjo, A. M., Maharaj, S. D., & Moopanar, S. 2018, CQGra, 35, 045015
Manjonjo, A. M., Maharaj, S. D., & Moopanar, S. 2019, JPhCo, 3, 025003
Mathias, A. K., Maharaj, S. D., Sunzu, J. M., & Mkenyeleye, J. M. 2021, Prama, 95, 178
Matondo, K. D., Maharaj, S. D., & Ray, S. 2018, EPJC, 78, 437
Maurya, S. K., & Govender, M. 2017, EPJC, 77, 347
Maurya, S. K., & Maharaj, S. D. 2017, EPJC, 77, 328
Maurya, S. K., & Maharaj, S. D. 2018, EPJA, 54, 68
Moopanar, S., & Maharaj, S. D. 2013, JEnMa, 82, 125
Murad, M. H. 2016, Ap&SS, 361, 20
Murad, M. H. 2018, EPJC, 78, 285
Murad, M. H., & Fatema, S. 2015, EPJC, 75, 533
Ngubelanga, S. A., Maharaj, S. D., & Ray, S. 2015, EPJP, 130, 211
Pandey, S. N., & Sharma, S. P. 1982, GReGr, 14, 113
Pandya, D. M., & Thomas, V. O. 2019, CaJPh, 97, 3
Rahaman, F., Maulick, R., Yadav, A. K., Ray, S., & Sharma, R. 2012, GReGr, 44, 107
Schwarzschild, A. 1916, Sitzer. Preuss. Akad. Wiss. Berlin, 424, 189
Sharma, R., & Ratanpal, B. S. 2013, IJMPD, 22, 1793
Singh, K. N., Murad, H. M., & Pant, N. 2017a, EPJA, 53, 21
Singh, K. N., Pant, N., & Govender, M. 2017b, EPJC, 77, 100
Stephani, H., Kramer, D., MacCallum, M. A. H., Hoenselaers, C., & Herlt, E. 2003, Exact Solutions of Einstein's Field Equations (2nd ed.; Cambridge: Cambridge Univ. Press)
Sunzu, J. M., Maharaj, S. D., & Ray, S. 2014a, Ap&SS, 352, 719
Sunzu, J. M., Maharaj, S. D., & Ray, S. 2014b, Ap&SS, 354, 517
Sunzu, J. M., & Mashiku, T. 2018, Prama, 91, 75
Sunzu, J. M., Mathias, A. K., & Maharaj, S. D. 2019, JApA, 40, 8
Thirukkanesh, S., & Maharaj, S. D. 2008, CQGra, 25, 235001
Thirukkanesh, S., & Ragel, F. C. 2012, Prama, 78, 687
Tolman, R. C. 1939, PhRv, 55, 364